A Comparative Study of Approximate Treatments of the Density Polarization in CN^- *

Marek Koniński and Roman F. Nalewajski

Department of Theoretical Chemistry, Jagiellonian University, Cracow, Poland

Z. Naturforsch. **43a**, 228–232 (1988); received November 21, 1987

The simple perturbative description of the main polarization effects in molecular systems is tested and calibrated using the modified Hamiltonian MNDO SCF results for the cyano group CN^- perturbed by positive or negative point charges. The relative importance of various polarization channels is examined and the reliability of the MNDO predictions is investigated by testing them against the respective ab initio modified Hamiltonian results. It is shown that the δ-function approximation of the point-charge perturbative potential leads to semiquantitatively correct density relaxation patterns, already within one-channel approximation.

1. Introduction

The knowledge of the main electronic density relaxation effects is of vital importance for an understanding of the chemical reactivity [1–4]. The electrostatic and polarization interactions determine the relative approach of reactants at an early stage of a reaction (before the charge transfer and molecular rearrangement), at distances at which the approximation of "small" (or negligible) "orbital overlap" is valid. We have recently reported a simple, qualitative analysis of the density polarization effects [5], which allows a qualitative prediction of the main trends in the density relaxation for both the single and multiple site reactivity cases. Although correct qualitative polarization trends have been predicted for selected molecular systems, more detailed quantitative comparison with the modified hamiltonian SCF results is necessary to estimate the relative importance of various polarization channels (transition densities).

It is the main purpose of this paper to perform such an evaluation of the reliability of this approximate treatment. We do this by calibrating this approach, using the modified Hamiltonian (MH) MNDO SCF results for the cyano group, CN^-, perturbed by positive or negative point charges, simulating the electrostatic perturbation in various R...CN and CN...R compounds. We also demonstrate the reliability of the MH MNDO predictions by showing the overall parallelism between the present MH MNDO results and the previously reported [6] ab initio MH SCF results. To facilitate this comparison the positions and values of perturbing charges [on the CN (z)-axis, on both sides of CN^-] were taken from [6].

* This work was supported by a grant from the Institute of Low Temperatures and Structural Research, Polish Academy of Sciences, Wrocław (Program CPBP 01.12) and a grant from the Institute of Physical Chemistry, Polish Academy of Sciences, Warsaw (Program CPBR 3.20).

Reprint requests to Doc. Dr. R. F. Nalewajski, Department of Theoretical Chemistry, Jagiellonian University, Karasia 3, 30-060 Kraków/Polen.

2. Calculations and Results

The placing of a molecule in the electrostatic potential generated by a point charge Z (atomic units are used throughout the paper) at position $\boldsymbol{D}$ modifies the unperturbed molecular Hamiltonian $\hat{H}$,

$$\hat{H}(\boldsymbol{D}) = \hat{H} - \sum_{i=1}^{N} Z/(\boldsymbol{r}_i - \boldsymbol{D}) \equiv \hat{H} + \hat{V}(\boldsymbol{D}), \qquad (1)$$

where N is the number of valence electrons. Introducing into the MNDO core Hamiltonian the corresponding matrix elements of the perturbing field, estimated in accordance with the usual Goeppert-Mayer and Sklar approximation (with neglect of penetration integrals) gives the MH MNDO SCF method for N valence electrons.

The second-order molecular orbital (MO) perturbation theory gives the change in the electron density, $\delta n^*(\boldsymbol{r})$, as the sum of contributions from various transition densities, Ω_k,

$$\delta n^*(\boldsymbol{r}) = -4 \sum_k [V_k(\boldsymbol{D})/\Delta e_k]\, \Omega_k(\boldsymbol{r}) \equiv -4 \sum_k \lambda_k(\boldsymbol{D})\, \Omega_k(\boldsymbol{r}), \qquad (2)$$

0932-0784 / 88 / 0300-0228 $ 01.30/0. – Please order a reprint rather than making your own copy.

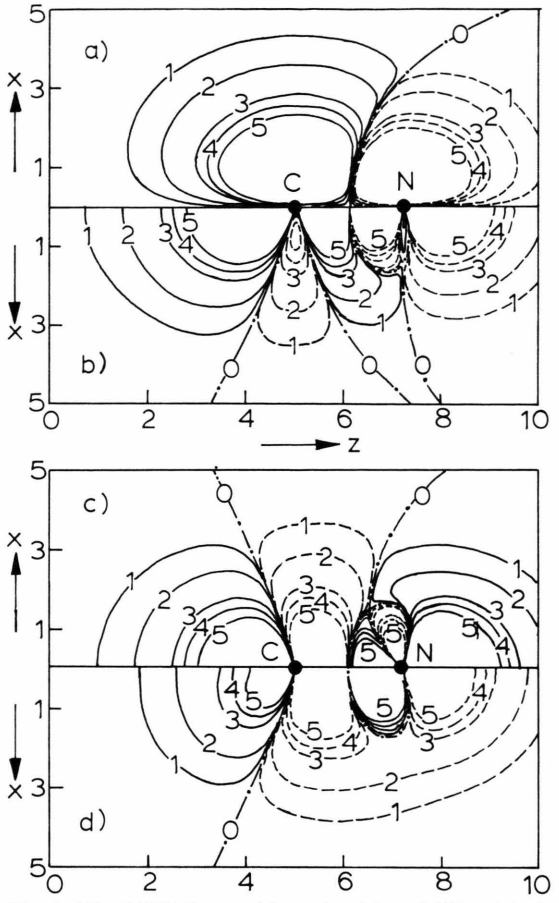

Fig. 1. The MNDO transitions densities of CN^-: (a) $\pi_1^x \pi_3^x$; (b) $\sigma_3 \sigma_4$; (c) $\sigma_2 \sigma_4$; (d) $\sigma_1 \sigma_4$. The solid lines correspond to the positive contour values while the broken lines represent the negative values. The magnitudes of the contours are: $1 - 10^{-5}$. $2 - 10^{-4}$, $3 - 10^{-3}$, $4 - 2 \times 10^{-3}$, $5 - 4 \times 10^{-3}$. The same values are used in all contour maps of Figures 1–4.

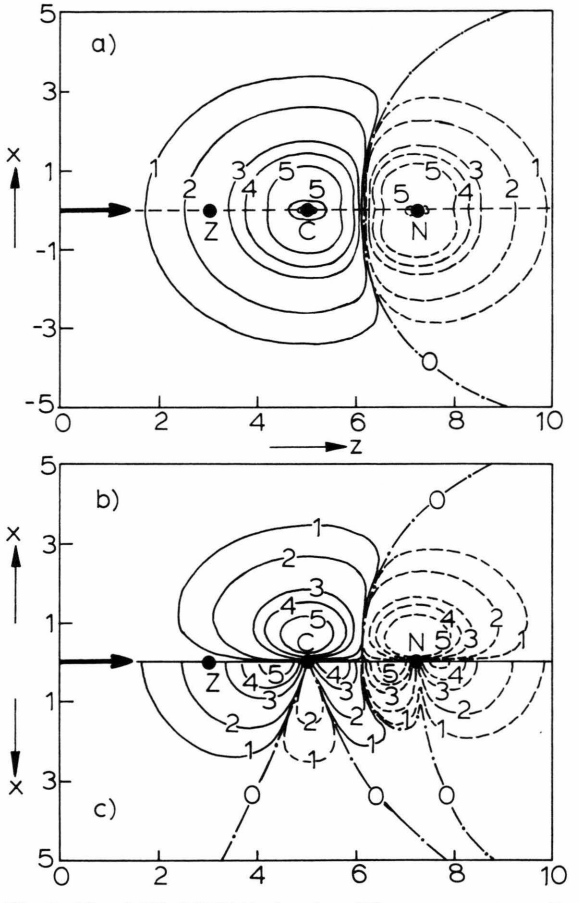

Fig. 2. The MH MNDO density difference contour diagrams for the $e(0.4) - C = 2$ attack: (a) total density; (b) π-electron density; (c) σ-electron density.

where $\Delta e_k \equiv \Delta e_{ij} = e_j - e_i$ is the difference in the MO energy levels, $V_k(\boldsymbol{D}) \equiv V_{ij}(\boldsymbol{D}) = \langle \Psi_i | \hat{V}(\boldsymbol{D}) | \Psi_j \rangle$, and $\Omega_k \equiv \Psi_i \Psi_j$ represents the "polarization channel" resulting from the $\Psi_i \Rightarrow \Psi_j$ "excitation" from the i-th (occupied) to j-th (virtual) MO's.

Within the minimal basis set calculations and the positions of the approaching charge on the bond axis, there are possible three $\sigma_i \Rightarrow \sigma_j$ and one $\pi_1^x \Rightarrow \pi_3^x$ (or $\pi_2^y \Rightarrow \pi_4^y$) excitations. The corresponding transition densities are shown in Figure 1.

In Fig. 2a we present the total MH MNDO density change, δn^*, generated by an electrophilic (e) attack of a charge $Z = +0.4$ placed on the bond axis on the carbon (C) side in the R_{ZC} distance of 2 a.u.; in short we denote such an approach using the following notation: $e(0.4) - C = 2$. Figure 2b shows the respective π-electron density change, δn_π^*, for the same perturbation. The corresponding δn_σ^* contribution is given in Figure 2c.

In order to evaluate the relative significance of three possible σ polarization channels we have fitted the one- and two-channel polarized molecular orbitals, $\sigma_i(\lambda_1)$, $\sigma_i(\lambda_1, \lambda_2)$, to the exact (three-channel) MH MNDO polarized MO's, σ_i^*, using the Maximum Overlap Criterion (MOC).

Let us first consider the simplest one-channel polarization of σ_3 and σ_4:

$$\sigma_3(\lambda_1) = N_1(\sigma_3 - \lambda_1\sigma_4) \approx \sigma_3^*,$$
$$\sigma_4(\lambda_1) = N_1(\sigma_4 + \lambda_1\sigma_3) \approx \sigma_4^*, \quad (3)$$

where $N_1 = (1 + \lambda_1^2)^{-1/2}$. The optimum MOC fit of λ_1 follows from the criterion:

$$\max_{\lambda_1'} [\langle\sigma_3(\lambda_1')|\sigma_3^*\rangle + \langle\sigma_4(\lambda_1')|\sigma_4^*\rangle] \Rightarrow \lambda_1. \quad (4)$$

The resulting one-channel $(\sigma_3\,\sigma_4)$ fits of the σ polarization maps for the $e(0.4) - C = 2$ and $e(0.4) - N = 2$ attacks are shown in Figs. (3c) and (4c) respectively.

We have also determined the optimum two-channel $(\sigma_2\,\sigma_4, \sigma_3\,\sigma_4)$ approximations to σ_2, σ_3 and σ_4 MO's:

$$\sigma_2(\lambda_1) = N_1(\sigma_2 - \lambda_1\sigma_4) \approx \sigma_2^*,$$
$$\sigma_3(\lambda_2) = N_2(\sigma_3 - \lambda_2\sigma_4) \approx \sigma_3^*, \quad (5)$$
$$\sigma_4(\lambda_1, \lambda_2) = N_3(\sigma_4 + \lambda_1\sigma_2 + \lambda_2\sigma_3) \approx \sigma_4^*,$$

where, $N_1 = (1 + \lambda_1^2)^{-1/2}$, $N_2 = (1 + \lambda_2^2)^{-1/2}$, and $N_3 = (1 + \lambda_1^2 + \lambda_2^2)^{-1/2}$, using the MOC criterion:

$$\max_{\lambda_1', \lambda_2'} [\langle\sigma_2(\lambda_1')|\sigma_2^*\rangle + \langle\sigma_3(\lambda_2')|\sigma_3^*\rangle + \langle\sigma_4(\lambda_1', \lambda_2')|\sigma_4^*\rangle]$$
$$\equiv \max_{\lambda_1', \lambda_2'} O(\lambda_1', \lambda_2') \Rightarrow (\lambda_1, \lambda_2). \quad (6)$$

The extremum principle (6) leads to the system of coupled nonlinear equations:

$$\partial O/\partial\lambda_1' = 0 \quad \text{and} \quad \partial O/\partial\lambda_2' = 0, \quad (7)$$

which have been solved numerically. The corresponding two-channel fits of the σ-electron polarization maps are shown in Figs. (3b) and (4b).

Yet another two-channel fit has been determined for the δ-function approximation of the perturbing potential.

$$Z/|\boldsymbol{r} - \boldsymbol{D}| \approx q\,\delta(\boldsymbol{r} - \boldsymbol{D}), \quad (8)$$

which we have previously adopted in a qualitative analysis of polarization effects [5]. This approximation expresses λ_1 and λ_2 as known functions of the common parameter q (a measure of the effective perturbing charge),

$$\lambda_1 = -q\,\Omega_{2,4}^{\sigma}/\Delta e_{2,4}^{\sigma} \equiv \lambda_1(q),$$
$$\lambda_2 = -q\,\Omega_{3,4}^{\sigma}/\Delta e_{3,4}^{\sigma} \equiv \lambda_2(q). \quad (9)$$

The equation to be solved numerically is:

$$\mathrm{d}O[\lambda_1(q), \lambda_2(q)]/\mathrm{d}q = 0. \quad (10)$$

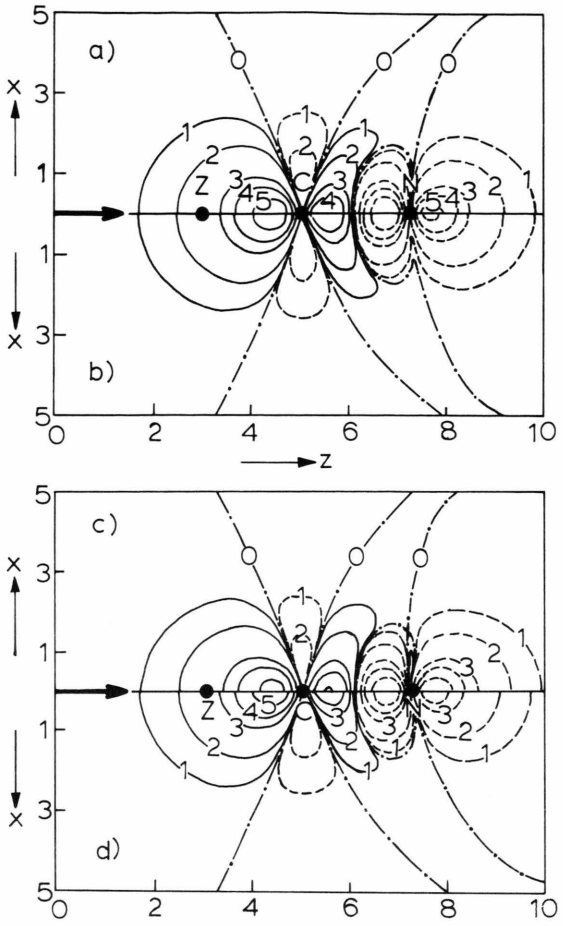

Fig. 3. A comparison of the σ-electron density difference maps for the $e(0.4) - C = 2$ attack: MH MNDO; MOC fit of the $(\sigma_3 \Rightarrow \sigma_4,\ \sigma_2 \Rightarrow \sigma_4)$ two channel polarization; (c) MOC fit of the $\sigma_3 \Rightarrow \sigma_4$ one channel polarization; (d) MOC fit of the $(\sigma_3 \Rightarrow \sigma_4, \sigma_2 \Rightarrow \sigma_4)$ two-channel polarization within the δ-function approximation.

The two polarization maps corresponding to this two-channel approximation are shown in Figs. (3d) and (4d).

In Table 1 we compare the optimum estimates of the coupling matrix elements for σ MO's, resulting from the MOC criterions described above.

As mentioned in the Introduction the CN^- case has been selected to facilitate the comparison between the MH MNDO and MH ab initio SCF polarization trends. In Fig. 5 we present such a comparison of changes in the σ_3 (a) and π_1 (b) MO energy levels, and the gross atomic electron populations (c), for various perturbations considered in [6].

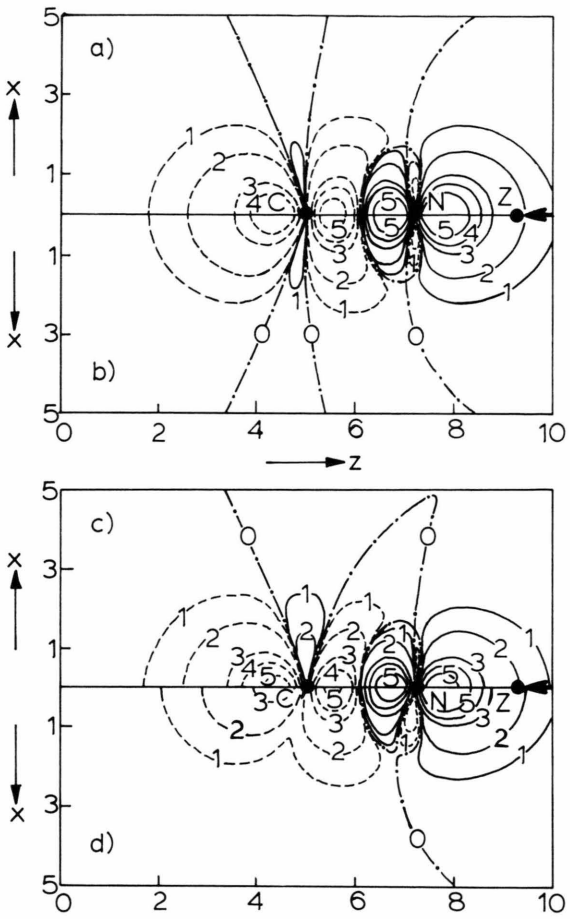

Fig. 4. A comparison of the σ-electron difference maps for the $e(0.4) - N = 2$ attack (see the legend of Fig. 3 for the explanation of the (a–d) approximations).

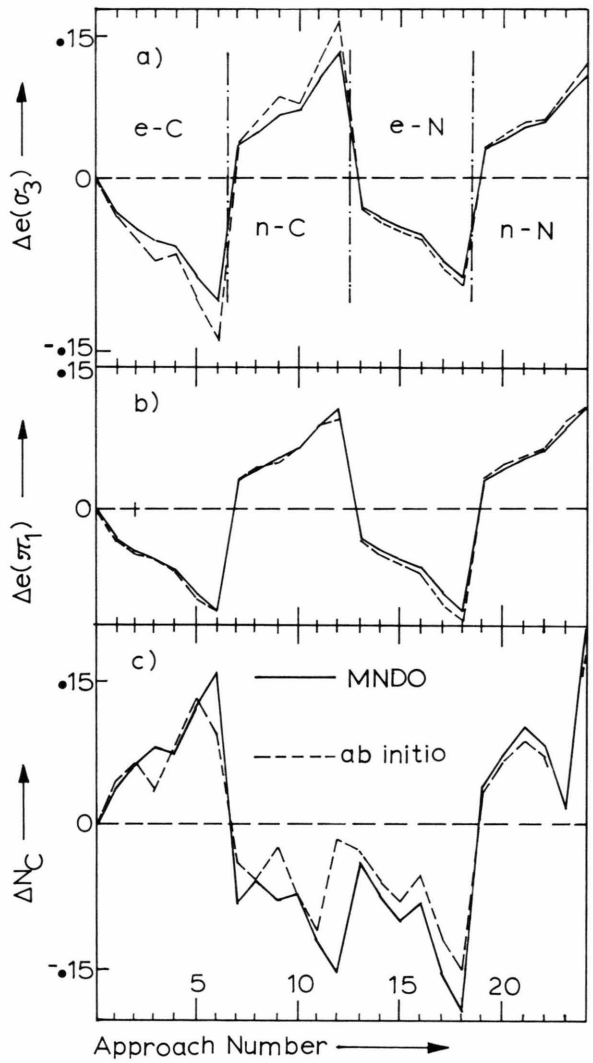

Fig. 5. A comparison of the MH ab initio and MH MNDO polarization changes for CN^-: variations in MO energies of the highest occupied $\sigma(\sigma_3, a)$ and $\pi(\pi_1, b)$ orbitals, and variations in the gross atomic populations on carbon atom (c). The specifications of the approach numbers are the following: $1: e(0.2) - C = 5$; $2: e(0.2) - C = 3$; $3: e(0.2) - C = 2$; $4: e(0.4) - C = 5$; $5: e(0.4) - C = 3$; $6: e(0.4) - C = 2$; $7: n(-0.2) - C = 5$; $8: n(-0.2) - C = 3$; $9: n(-0.2) - C = 2$; $10: n(-0.4) - C = 5$; $11: n(-0.4) - C = 3$; $12: n(-0.4) - C = 2$; $13: e(0.2) - N = 5$; $14: e(0.2) - N = 3$; $15: e(0.2) - N = 2$; $16: e(0.4) - N = 5$; $17: e(0.4) - N = 3$; $18: e(0.4) - N = 2$; $19: n(-0.2) - N = 5$; $20: n(-0.2) - N = 3$; $21: n(-0.2) - N = 2$; $22: n(-0.4) - N = 5$; $23: n(-0.4) - N = 3$; $24: n(-0.4) - N = 2$. The e – C notation represents an electrophilic attack on the carbon side, n – N stands for the nucleophilic perturbation on the nitrogen side, etc.

Table 1. Comparison of the coupling matrix elements between σ MO's for the $e(0.4) - C = 2$ (a), and $e(0.4) - N = 2$ (b) perturbations

Matrix element	Approximation			
	MH MNDO	MOC 2-channels	MOC 1-channel	MOC, 2-channels δ-approximation
	a) e – C			
$\langle\sigma_3\|\hat{V}\|\sigma_4\rangle$	−0.401	−0.463	−0.462	−0.448
$\langle\sigma_2\|\hat{V}\|\sigma_4\rangle$	0.203	0.171		0.231
	b) e – N			
$\langle\sigma_3\|\hat{V}\|\sigma_4\rangle$	0.494	0.454	0.454	0.342
$\langle\sigma_2\|\hat{V}\|\sigma_4\rangle$	0.180	0.335		0.472

3. Discussion

The four modes of density redistribution represented by the transition densities of Fig. 1 have their respective contributions to δn^* (Fig. 2a) inversely proportional to the corresponding differences in the orbital energies, Δe_{ij} [Eq. (2)]. This energetical factor increases in the sequence of channels: $\pi_1\pi_3$, $\sigma_3\sigma_4$, $\sigma_2\sigma_4$, $\sigma_1\sigma_4$ (Figs. 1a–d): 0.556, 0.701, 0.910, and 1.612, respectively. In the qualitative δ-function approximation [Eq. (8)] the coupling matrix element $\langle\psi_i|\hat{V}(\boldsymbol{D})|\psi_j\rangle$ is proportional to $\Omega_{ij}(\boldsymbol{D})$, the transition density at the position $\boldsymbol{D}$ of the approaching charge Z. For the attacks along the bond axis $\Omega_{ij}(\boldsymbol{D})$ is the largest for the σ-channels, with the maximum values for the two lowest channels (Figures 1b, c). For the π-channel having $\Omega(z=0)=0$ such an approximation obviously fails. In Table 1 we present various estimates of the coupling matrix elements between the σ MO's for the attacks of Figs. 3 and 4.

The π polarization channel effects the electron flow between both atoms in the region away from the bond axis (compare Figs. 1a and 2b). The σ polarization channels have their maxima on the bond axis, thus leading to the dominating contribution in the region around the bond axis (Figure 2c). The resultant effect (Fig. 2a) is a shift of electrons from one atom to another. Notice that the σ contribution to $\mathrm{d}n^*$, $\mathrm{d}n^*_\sigma$, basically describes a transfer of electrons between the $s^a p_z^b$ hybrid orbitals on both atoms, directed towards both possible directions of an attack. Notice also, that when an electrophile approaches carbon there is also a slight intra-atom density rearrangement on the carbon atom, leading to a flow of electrons from the region perpendicular to the bond, with the most of the charge being directed towards the perturbing positive charge.

It should be noticed that there is a close resemblance between the $\mathrm{d}n^*_\pi$ (Fig. 2b), $\mathrm{d}n^*_\sigma$ (Fig. 2c) density difference plots and the transition densities $\pi_1\pi_3$ (Fig. 1a), $\sigma_3\sigma_4$ (Fig. 1b), respectively, thus showing that both the π and σ polarization trends are dominated by the frontier MO's for each symmetry type. This conclusion is more quantitatively tested for the δn^*_σ case in Figs. 3 and 4.

Figures 3 a, b and 4 a, b, for the electrophilic attacks towards C (e – C) and N (e – N), respectively, demonstrate that the exact (three-channel) density difference maps (Figs. 3a and 4a) are almost perfectly reproduced by the two-channel MOC fits. However, the one-channel MOC fits (Figs. 3c and 4c) also constitute a remarkably good representations of the overall σ density difference maps, thus showing the dominant role of the σ frontier MO polarization channel.

Figures 3d and 4d test the adequacy of the relative weights of vaurious channels determined by δ-function approximation. Notice that with the MOC effective charges the predicted density difference maps are also in surprisingly good agreement with the exact σ polarization maps. This quantitatively demonstrates the soundness of such an approximation in an analysis of the density relaxation patterns and supplements our previous qualitative demonstration [5]. Reference to Figs. 3 and 4 also shows that the predictions are slightly better in the case of the e – C approach in comparison with the e – N attack.

It can be seen in Table 1 that the MH MNDO coupling matrix elements between σ MO's are generally well reproduced within one- and two-channel MOC fits. The same conclusion applies to the two-channel δ-function approximation approach. However, in the case of the e – N attack the relative values for the $\sigma_3\sigma_4$ and $\sigma_2\sigma_4$ channels are reversed in the δ-function approximation.

It should be emphasized, however, that the similar values of the matrix element do not necessarily imply the similar values of the MOC q values in the δ-function approximation [Eq. (8)], since they must strongly depend on the values of the transition densities at the position of the polarizing charges, $\Omega_k(D)$. For example, the q values for the e – C, e – N approaches of Figs. 3 and 4, respectively, are: 2.16 and 4.75.

It follows from Fig. 5 that the MH ab initio patterns of changes in the σ and π highest occupied MO's, as well as these of variations in atomic electron populations, are all very well reproduced in the MH MNDO method using the Goeppert-Mayer and Sklar approximation. The changes in MO energy levels (Figs. 5a, b) are predicted with slightly higher accuracy than those in atomic populations (Fig. 5c), where more pronounced deviations can be observed.

[1] K. N. Houk, Topics in Current Chemistry, Organic Chemistry, Vol. 79; Springer-Verlag, Berlin 1979, p. 1, and refs. therein.
[2] R. J. Bartlett and H. Weinstein, Chem. Phys. Lett. **30,** 441 (1975).
[3] H. Weinstein, Intern. J. Quantum Chem. QBS **2,** 59 (1975); S. Y. Chang, H. Weinstein and D. Chou, Chem. Phys. Letters **42,** 145 (1976).
[4] H. Weinstein, J. E. Eillers, and S. Y. Chang, Chem. Phys. Letters, **51,** 534 (1977).
[5] R. F. Nalewajski and M. Koniński, Z. Naturforsch. **42a,** 451 (1987).
[6] E. Clementi and D. Klint, J. Chem. Phys. **50,** 4899 (1969).